Resonance emission spectroscopy of predissociating SO_2 $\tilde{C}(1\,^1B_2)$: Coupling with a repulsive $^1A_1$ state near 200 nm

Paresh C. Ray, Michael F. Arendt, and Laurie J. Butler
The James Franck Institute and the Department of Chemistry, The University of Chicago, Chicago, Illinois 60637

(Received 7 May 1998; accepted 26 June 1998)

This work investigates the predissociative $\tilde{C}(1^1B_2)$ state of SO_2 by cooling the SO_2 in a pulsed molecular beam and dispersing the emission upon resonant excitation into several different vibronic absorption features in the $\tilde{C}$ state between 197 and 212 nm. Unlike at the lower excitation energies, the dispersed emission spectra at the higher excitation energies are dominated by progressions with odd quanta in the antisymmetric stretch mode ν_3 and combination bands with up to six quanta in the bending mode ν_2. The formidable intensity for emission into vibrational states with odd quanta in the antisymmetric stretch of the jet-cooled molecule suggests that the intermediate state at high energies in the excited state is of mixed electronic character at nonsymmetric geometries, so the operative components of the transition moment for excitation and emission may be different. We discuss our results by considering the avoided crossing seam and coupling between the $\tilde{C}(1^1B_2)$ state and two dissociative states potentially involved in the electronic predissociation, the $3\,^1A_1$ and the $1\,^3A_1$ states. © *1998 American Institute of Physics.* [S0021-9606(98)02037-6]

I. INTRODUCTION

The importance of sulfur dioxide (SO_2) as an atmospheric trace species, primarily from coal combustion processes, and as a constituent of the atmosphere of Venus has made it the subject of photochemical study for many years.[1–14] The ground state of SO_2 is $\tilde{X}(^1A_1)$ with an equilibrium O–S–O angle of 119.5 deg and an equilibrium S–O bond distance of 1.432 Å. The photodissociation reaction initiated in the structured electronic absorption band beginning near 235 and peaking near 200 nm has been ascribed to predissociation from the $\tilde{C}(1\,^1B_2)$ state to produce the ground-state products $SO(^3\Sigma^-)+O(^3P)$.

Katagiri *et al.*[14] reviewed the previous work on SO_2 in the $\tilde{C}$ state in 1997, so we give only a brief account here. Several experimental studies have investigated the onset of predissociation and sought to understand the mechanism at energies near the onset.[4–7] Okabe[4] first observed absorption and fluorescence excitation spectra of the $\tilde{C}\leftarrow\tilde{X}$ transition under bulb conditions at room temperature and showed clearly that the fluorescence intensity drops abruptly for excitation wavelengths below 218.9 to 220.8 nm, while the strong absorption is maintained with clear vibrational structure after 219 nm. The predissociation threshold for the $SO(^3\Sigma^-)+O(^3P)$ asymptote was estimated to be located at 219 nm (5.66 eV), consistent with the dissociation energy, $D_e=5.65\pm.01$ eV, estimated using thermochemical data. On the other hand, Ebata *et al.*[5] find a lower energy onset for the predissociation. They observed the laser-induced fluorescence (LIF) spectrum of jet-cooled SO_2 and reported the predissociation threshold at 45 400 cm^{-1} (220 nm). Ivanco *et al.*[7] measured the fluorescence decay curves upon excitation in the $\tilde{C}\leftarrow\tilde{X}$ transition of jet-cooled SO_2 and argued that the onset of the predissociation is located at 218.0 nm, since the quantum beat in the fluorescence decay disappears for the 218.0-nm transition.

In the last two decades, several studies[8–19] have investigated the mechanism of predissociation of SO_2 at both lower and higher energies in the $\tilde{C}$ state. The interesting feature of the $\tilde{C}\leftarrow\tilde{X}$ band of SO_2 is that vibronic absorption features with rotationally resolved structure can be observed even above the dissociation threshold for the $SO(^3\Sigma^-)+O(^3P)$ asymptote located in the middle of the Franck–Condon region (235–165 nm). Freeman *et al.*[9] measured the absorption spectrum of the $\tilde{C}\leftarrow\tilde{X}$ band of cold SO_2 vapor at 213 K in a wide range covering the wavelength region between 240 and 170 nm with high resolution (0.002 nm) and determined the absolute absorption cross section. The quantum beat phenomena observed by Ivanco *et al.*[7] above 218 nm was ascribed to the vibronic coupling with nearby vibrational levels of the electronic ground state $\tilde{X}(1\,^1A_1)$. It was suggested that the predissociation would proceed via vibronic coupling with the highly excited quasibound vibrational levels in the $\tilde{X}$ state. However, a triplet mechanism was supported by the work of Ebata *et al.*[5] The (3,0,0) absorption band (3 quanta in symmetric stretch) at the onset of predissociation showed that the $J=K$ levels of the Q-branch were anomalously strong in the fluorescence excitation spectrum, supporting the hypothesis that SO_2 predissociates via a crossing with a triplet state. They also found that the fluorescence lifetime for the low rotational levels of the bands above 45 600 cm^{-1} was longer than that of the high rotational levels, concluding that the high rotational levels predissociated faster than the low rotational levels. Vibrational states with two quanta in the antisymmetric stretch in the $\tilde{C}$ state predissociated faster than those with zero quanta in ν_3. Hui *et al.*[6] measured the fluorescence lifetime of the $\tilde{C}$ state and found that the life-

time is 45 ns at 221 nm and decreases to 8 ns at 215 nm. Katagiri *et al.*[14] greatly extended these measurements, deducing the predissociation rates from quantum yield measurements for 30 vibronic levels in the $\tilde{C}$ state between 220 and 200 nm, and showing the predissociation rate increases roughly exponentially from near a nsec at 215 nm to 10 psec (or 100 psec using linewidth measurements) near 200 nm. Okazaki *et al.*[12] studied the low energy region of the absorption spectrum, tuning into various vibronic features in the $\tilde{C}$ state of SO_2, and concluded that the antisymmetric stretch ν_3 mode served as a promoting mode for the internal conversion to the $\tilde{X}$ state. The vibronic level dependence of the rise time of the O atom product was in accord with that of the fluorescence lifetime, and so they concluded that the predissociation proceeds by internal conversion to the ground state. Abe and Hayashi[8] investigated the fluorescence quenching due to an external magnetic field of the $\tilde{C} \leftarrow \tilde{X}$ vibronic bands in the energy region below the dissociation threshold and found some contribution from vibronic mixing between the $\tilde{C}$ state and a nearby singlet state.

Several studies have detected the photofragments from SO_2 $\tilde{C}$ state predissociation at 193 nm, offering further insight into the predissociation mechanism operative at this wavelength.[10–11,15–17] Kawasaki *et al.*[10] measured the translational energy and angular distribution of the SO photofragments for the 193 nm photodissociation of SO_2 in a molecular beam; their kinetic energy distribution was further refined by Felder *et al.*[16] The isotropic angular distribution indicated the dissociation lifetime was greater than a picosecond, in agreement with the estimates from fluorescence studies. However, the high recoil kinetic energies indicated that the dominant dissociation mechanism at 193 nm is via predissociation of the $\tilde{C}$ state by a crossing with a repulsive electronic state, not internal conversion to the ground electronic state. Kawasaki *et al.*[10] estimated the barrier to the reverse reaction (the so-called exit barrier), e.g., barrier energy from the asymptotic product to the avoided crossing, to be 2500 cm^{-1}. They attributed the barrier to a crossing with a repulsive triplet state, although the kinetic energy measurements are consistent with a mechanism involving a repulsive singlet state. Based on the distribution of the spin-orbit sublevels of the SO photofragments, Kanamori *et al.*[11] suggested that the SO product in $v=1$ and 2 are formed through a crossing with a repulsive triplet state. However, in considering these results, note that the dominant dissociation mechanism can be different at higher excitation energies than at the onset of predissociation. Indeed, if the crossing with a repulsive singlet state were only accessible at higher energies than the asymptotic product limit, an internal conversion mechanism or a triplet mechanism could predominate at the lower excitation energies, while dissociation via an avoided crossing with a repulsive singlet state could contribute at higher excitation energies.

From the experimental studies above, it is clear that the predissociation mechanism is not so simple. Katagiri *et al.*[14] review the previous *ab initio* work relevant to the $\tilde{C}$ state predissociation in SO_2. There are a number of nearby electronic states which could possibly interact with the $\tilde{C}$ state to produce $SO(^3\Sigma^-)+O(^3P)$ photofragments. Kamiya *et al.*'s *ab initio* studies[13] of the excited states involved in the predissociation of the SO_2 $\tilde{C}(1\,^1B_2)$ state consider two mechanisms, one via spin-orbit coupling to the $2\,^3A'$ ($1\,^3A_1$ in C_{2v}) state at a state crossing and another mechanism via a higher energy avoided crossing with another singlet electronic state (which is a repulsive $^1A_1$ state in C_{2v}). Although higher level complete active space self-consistent field (CASSCF) and multireference configuration interaction (MRCI) calculations by Katagiri *et al.*,[14] freezing the r and θ Jacobi coordinates at the equilibrium geometry in the ground state, quote the crossing to be only narrowly avoided, with a splitting of less than 20 meV, and thus conclude the singlet mechanism must be a minor one, they do find the splitting at the singlet avoided crossing is as large as 0.1 eV at some geometries.

In this paper we have investigated the jet-cooled emission spectra of predissociating sulfur dioxide from excitation at energies ranging from the low energy region of the $\tilde{C}$ state absorption spectrum to the higher energy region near 200 nm. It has been shown that resonance Raman, or emission spectroscopy,[20–26] is a very powerful technique to examine the early time photodissociation dynamics of many molecular systems. (Here one might be tempted to call the emission fluorescence instead of resonance Raman since we tune the laser into vibrational features in the $\tilde{C}$ state, but the lifetimes decrease rapidly with excitation energy and number of quanta in the antisymmetric stretch, so are already less than 2 nsec at excitation energies near 47 000 cm^{-1} and 10 to 100 psec near 50 000 cm^{-1}.) Heller and co-workers[20,21] developed the early theoretical formalism for the time-dependent resonance and off-resonance Raman process. Kinsey and coworkers initiated the experimental work on directly dissociating molecules[22] and have reviewed[23] numerous other studies. Since the single excitation wavelength studies of Brand *et al.*,[27] the only dispersed emission studies on SO_2 near 200 nm, those of Yang and Myers,[26] were at a fixed wavelength near 210 nm, obtained by anti-Stokes shifting in H_2 the Nd:YAG fourth harmonic, and thus did not offer the possibility of tuning even into one resonance. This paper seeks to understand how the predissociation depends on the excitation energy and on the character of the vibronic level accessed. Thus we tune the energy of the excitation light into nine different vibronic features in the absorption spectrum between 212 and 197 nm and probe the early dynamics by measuring the emission spectrum from the predissociating molecules. (We also present one off-resonance emission spectrum in this energy region.)

II. EXPERIMENT

To obtain the excitation wavelengths between 197 and 212 nm, we used the doubled output of a Quantel YG 581-C Nd:YAG laser, with a pulse duration of 20 ns and pulse energy of 350 mJ, to pump a Lambda Physik F13002 dye laser at 20 Hz. The dye laser, tuned between 592 and 636 nm within the lasing range of Rhodamine 590, Rhodamine 610, Rhodamine 640, and DCM dyes, gives pulse energies between 30 and 40 mJ. An intercavity etalon reduces the band-

width to 0.05 cm^{-1}. We calibrate the dye laser with a Fisher Scientific Mg/Ne optogalvanic hollow cathode lamp. The output of the dye laser is then doubled in frequency via second-harmonic generation in a potassium-dihydrogen phosphate (KDP) crystal. After separating the visible and ultraviolet (UV) light with a dichroic beam splitter, the polarization of the visible light is rotated by a half-wave plate and then spatially recombined with the visible light with another dichroic beam splitter. The recombined light is then passed through a BBO crystal which generates the 197–212-nm beam (approximately 100–150 μJ pulse) via sum-frequency mixing of the visible with the frequency-doubled ultraviolet light.

The frequency-tripled output (197–212 nm) of the dye laser is first spatially separated from the residual visible and ultraviolet light with a Pellin-Broca prism and then passed through a stainless steel vacuum chamber where it photodissociates the SO_2 molecules. The neat SO_2 beam (99.5% purity, Matheson) is expanded at a stagnation pressure of 600 Torr through an IOTA-1 pulsed molecular beam valve with a 0.5-mm-diameter orifice. A standard broad range ion gauge is used to monitor the total chamber pressure prior to and during sample introduction. Ultimate background pressure within the chamber, pre sample introduction, is approximately 8.0×10^{-7} Torr. When the pulse molecular beam is operated at 20 Hz, the average pressure in the chamber rises to approximately 1×10^{-5} Torr and it remains constant during the experiment. The pulsed molecular beam valve is triggered sufficiently prior to the *Q*-switch of the YAG laser so as to assure that the valve has reached its maximum open position prior to interaction with light approximately 1 cm from the valve tip. The pulsed valve is allowed to remain open for 200 μs, assuring a well developed gas pulse. The laser pulse crosses the gas pulse about 100 μs after the leading edge of the gas pulse. Timing of the gas pulse with the tripled laser output is monitored using a homemade photodiode and Beam Dynamics fast ion gauge.

The emitted light from the predissociating SO_2 molecules is collimated, passed through a depolarizing wedge optic, and imaged onto the entrance slit (75 mm) of a Spectra-Pro 0.275 m spectrometer. The light is then dispersed by a 1200 grooves/mm Milton Roy holographic grating onto an EG&G 1455-B-700 HQ optical multichannel analyzer (OMA), which consists of an 18-mm photodiode array of 700 pixels, covering a 50-nm-wide emission spectrum. We give the dispersed emission spectra only to a Raman shift of 5000 cm^{-1} in this paper, as the spectra do not have unambiguous assignments at larger Raman shifts. The resolution of the OMA is limited by the grating, path length, and intensifier resolution (3 pixels) to 75 cm^{-1}. The detector is cooled to a temperature of -30 °C and the intensifier is gated by an amplified transistor–transistor logic pulse that is synchronized to the laser with a set delay from the Nd:YAG *Q*-switch. The OMA intensifier is ''on'' for only 200 ns around each laser pulse, so as to reduce the background noise from dark current in the photodiode array. The OMA is connected to an IBM-compatible computer which collects and displays the data. Each scan is collected for 100 s at 20 Hz, or approximately 2000 laser shots per scan. The spectra shown here are the sum of 75 scans or 150 000 laser shots. The calibration of the spectrometer grating position is fine tuned in these spectra with the literature values of the (0,1,0) and (0,0,1) bands of SO_2 at 517 and 1364 cm^{-1}.

III. RESULTS AND ANALYSIS

Jet-cooled resonance emission spectra of SO_2 excited at the vacuum wavelengths 197.7, 198.9, 201.8, 203.6, and 204.4 are presented in Fig. 1, and the resonance emission spectra excited at the vacuum wavelengths 205.1, 209.9, 210.6, and 211.5 nm are presented in Fig. 2. Figure 3 shows the emission spectrum obtained when you excite the SO_2 off-resonance in this wavelength region, at 208.7 nm (off-resonance). The excitation energy for each emission spectrum is converted to reciprocal centimeter units, properly accounting for the air to vacuum correction, and given in the top right of each emission spectrum. Band assignments are given as the number of quanta in the modes ν_1, ν_2, and ν_3, corresponding, respectively, to the symmetric stretch, bend, and antisymmetric stretch vibrational modes in the final electronic ground state. Assignments in Figs. 1–3 by A. Merer, private communication, are based on extrapolating progressions from the assigned infrared transitions in Shelton *et al.*[28] and the assigned dispersed emission bands by Brand *et al.*[27] Note that the resonances we are tuning into in the excited state for each of the emission spectra have not been assigned in this energy region of the $\tilde{C}$ state; Katagiri *et al.*[14] discuss some of the difficulties involved, such as a strong Fermi resonance between ν_1' and $2\nu_3'$ and the possible appropriateness of switching to assignments in terms of feature states.

The emission spectra reported here at excitation energies near the 200-nm absorption band are markedly different than the dispersed emission spectra recorded by other workers at lower excitation energies in the predissociative $\tilde{C}$ state of SO_2. This is evidence suggesting a distinct change in the predissociation dynamics in the excited state at high excitation energies as compared to low excitation energies. At low excitation energies, the emission spectra of Yang and Myers[26] at 234.9 and 223.1 nm (an excitation energy just below the onset of predissociation) evidence strong progressions in ν_2 and combination bands $\nu_1+n_2\nu_2$, but very little activity in ν_3. (Their spectrum reported at 208.9 nm is not on-resonance with an absorption feature.) Brand *et al.*[27] report the only emission spectrum at a higher excitation energy, from the 210.0-nm line of Zn(II). That spectrum still shows strong bands involving ν_1 and ν_2 as well as combination bands $n_1\nu_1+n_2\nu_2$, but also shows a significant progression in $n\nu_3$ and combination bands with both even and odd quanta in the antisymmetric mode ν_3. The lower two of our spectra in Fig. 2, bottom, at excitation energies near that of Brand, also evidence progressions in pure ν_1 and ν_2, and, like Brand, show considerable activity in combination bands of these with one quanta in ν_3. The only reported emission spectra at higher excitation energies (from 198 to 205 nm) in Fig. 2 top and in Fig. 1, however, show a marked change in which emission features dominate; in those spectra the bands involving ν_1 become increasingly less important with increasing excitation energy and the bands with odd quanta in

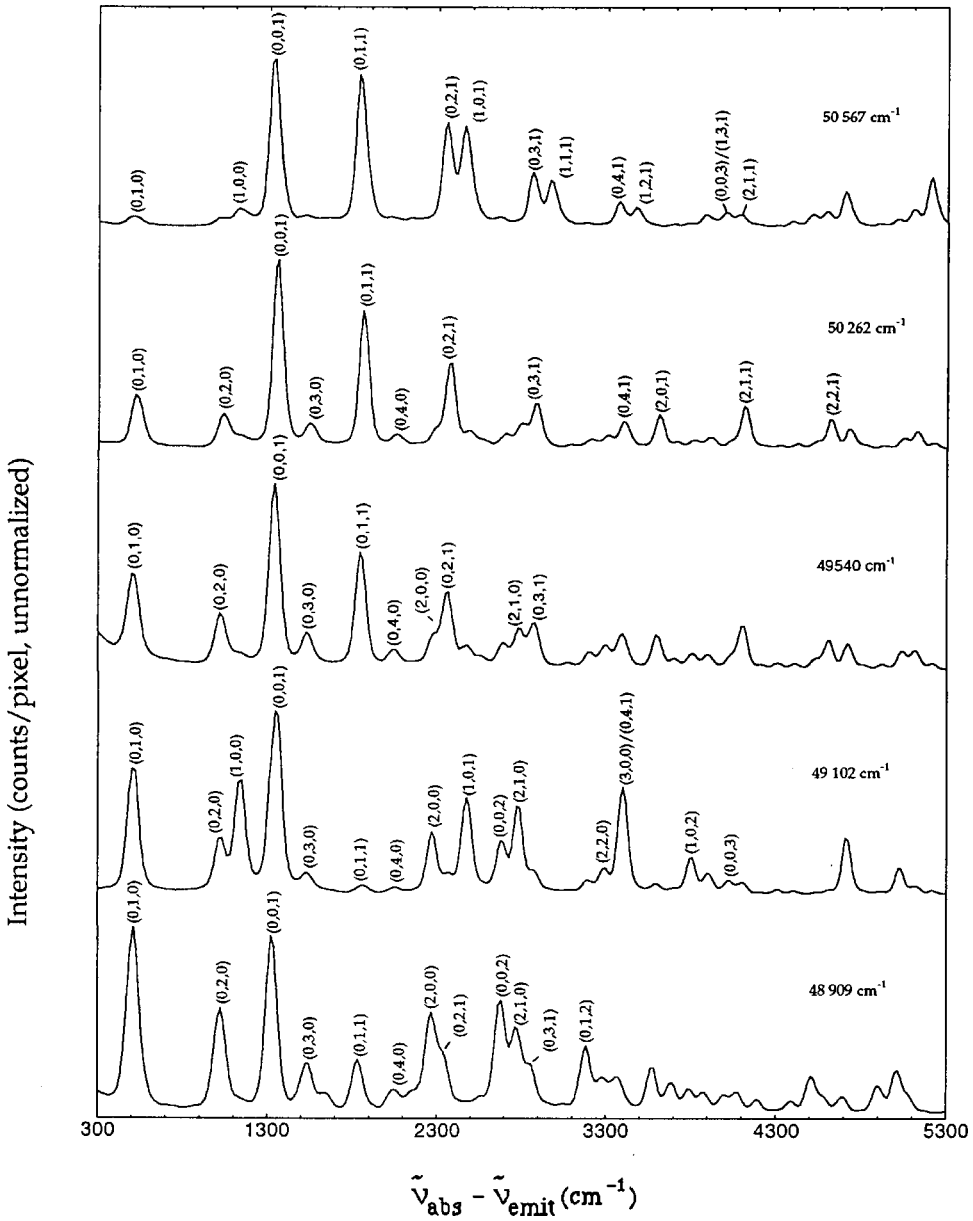

FIG. 1. Dispersed emission spectrum of predissociating SO_2 excited at 50 567 cm^{-1} (197.7 nm), (top); 50 262 cm^{-1} (198.9 nm); 49 540 cm^{-1} (201.8 nm); 49 102 cm^{-1} (203.6 nm); and 48 909 cm^{-1} (204.4 nm), (bottom). The assignment of the final state vibrational character in the $\tilde{X}$ state follows the notation of Ref. 27, where n_1 is the number of quanta in the symmetric stretch mode (ν_1), n_2 is the number of quanta in the bend mode (ν_2), and n_3 is the number of quanta in the antisymmetric stretch mode (ν_3). Peaks are labeled according to the convention (n_1,n_2,n_3).

ν_3 become increasingly more important. The spectra evidence emission into progressions in ν_2, the bending mode, both pure ν_2, and in combination with one quanta in ν_3, the antisymmetric stretching mode. The relative contribution of the pure ν_2 progression versus the ν_2 progression in combination with 1 quanta of ν_3 changes rapidly with excitation energy. The pure ν_2 progression is of comparable intensity to the combination band progression at the lowest of these high excitation energies (Fig. 2 top spectrum, 48 742 cm^{-1}, 205 nm) but the progression in ν_2 in combination with 1 quanta in ν_3 gains in importance as the excitation energy nears 200 nm, and dominates the 198 nm spectrum in Fig. 1, top. Clearly the dynamics in the excited state is very much different at higher excitation energies near 200 nm than near the predissociation onset of 219 nm. While at all excitation energies the spectra show considerable activity in the bend, showing the molecule is sampling regions of the excited state surface which are considerably removed from the Franck–Condon region in the bend normal coordinate, at the higher excitation energies the spectra also evidence an increasingly dominant contribution from motion in the antisymmetric stretch normal coordinate, q_3, on the excited state surface. The activity in the bend and in at least the even quanta in antisymmetric stretch are in apparent accord with *ab initio* calculations[14] and literature experimental values of the equilibrium bond distances and bond angles in the $\tilde{X}$ and $\tilde{C}$ states of SO_2. The equilibrium S–O bond distance for the ground state is 1.468 Å (experimental determined value is 1.43 Å) and the O–S–O bond angle is 122 deg (experimental value is 119.5 deg). In the $\tilde{C}$ state the two S–O equilibrium bond distances are different, 1.518 (experimental[27(b)] value 1.491) and 1.835 (experimental[27(b)] value 1.639 Å) respectively, and the bond angle is 108.3 deg (experimental[27(b)] value 103.75 deg). In the next paragraph we consider in detail the appearance of emission features with both even and odd quanta in ν_3 in the progressions involving antisymmetric stretching, as

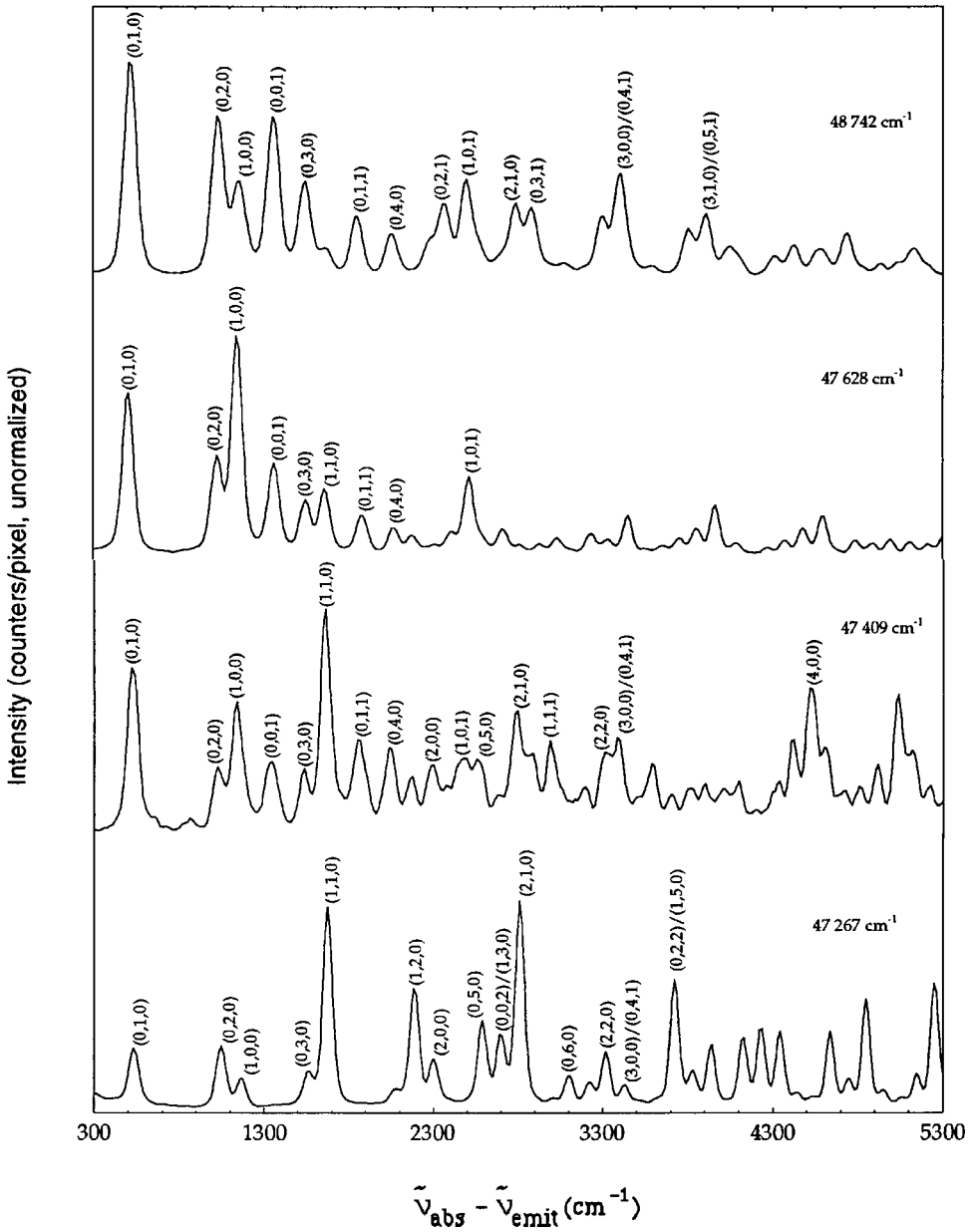

FIG. 2. Dispersed emission spectrum of predissociating SO_2 excited at 48 742 cm^{-1} (205.1 nm) (top); 47 628 cm^{-1} (209.9 nm); 47 409 cm^{-1} (210.6 nm); and 47 267 cm^{-1} (211.5 nm), (bottom). The assignment of the final state vibrational character in the $\tilde{X}$ state follows the notation of Ref. 27, where n_1 is the number of quanta in the symmetric stretch mode (ν_1), n_2 is the number of quanta in the bend mode (ν_2), and n_3 is the number of quanta in the antisymmetric stretch mode (ν_3). Peaks are labeled according to the convention (n_1,n_2,n_3).

it gives key information on why the excited state dynamics changes at the higher excitation energies.

The conclusion one can draw from the appearance of emission bands with odd quanta in ν_3'' are the same whether the emission process is more accurately described as fluorescence or, because of the picosecond predissociation times near 200 nm and the long coherence time of the excitation laser, as resonance Raman. Let us now consider the mechanisms that can lead to the appearance of emission into odd quanta in the antisymmetric stretch which are as strong as, or, in some spectra, stronger than the emission into bands with even quanta in ν_3''. At low excitation energies, Myers and Yang[26] do observe a small emission feature into the fundamental in ν_3. They state in their paper ''Strong transitions in the nominally forbidden odd quanta of ν_3 were also observed in the resonance fluorescence spectra of Brand *et al.*, who suggested a possible explanation involving strong

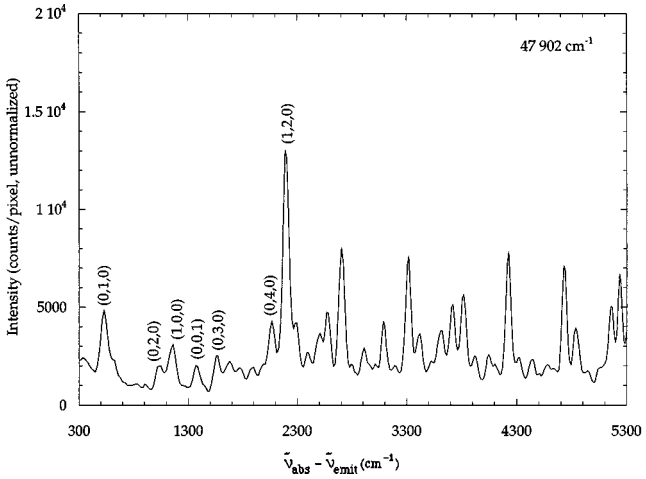

FIG. 3. Dispersed emission spectrum of predissociating SO_2 excited off-resonance at 47 902 cm^{-1} (208.7 nm).

Coriolis coupling in the excited electronic state.'' We need to now analyze the assumptions numerous workers make when they term these transitions ''nominally forbidden,'' as they are plainly strong in both our and Brand *et al.*'s spectrum. The first thing to note is that the mechanism for emission into odd quanta of ν_3 becoming allowed is certainly not Coriolis coupling, since our jet-cooled spectra show the emission into odd quanta in ν_3 as strong as in Brand's rotationally state-selected ($J_{K_{-1},K_1}=11_{1,10}$ in the intermediate excited state) spectra at similar excitation energies. Workers term the emission into odd quanta in ν_3 ''nominally forbidden'' because, like NO_2,[29] O_3,[30] and H_2S,[31] SO_2 has C_{2v} symmetry in the ground state. The first derivative of the upper state potential with respect to q_3 must vanish in the Franck–Condon region (indeed, the $\tilde{C}$ state potential has a double minimum at nonsymmetric geometries) and resonance Raman (or fluorescence) bands in ν_3 develop because the shape of the potential in excited states along q_3 differs from that in the ground state. In a wavepacket picture, the dynamics can spread and bifurcate the wavepacket in the intermediate excited state, but it cannot develop an *overall* non-C_{2v} symmetry (e.g., amplitude near one of the two double minima must be matched in absolute value by amplitude near the other). One must consider the global symmetry[32,33] of the excited electronic configuration state; the fact that the equilibrium geometry in the $^1B_2$ configuration state is at C_s geometries is irrelevant to the selection rules. We outline below how the commonly stated rule that only even quanta in antisymmetric stretching modes are allowed relies on the implicit assumption that the same component of the transition moment is operative for both the up transition (absorption) and the down transition (emission). (Note: The rule also typically relies on separating the rotational wavefunction from the vibronic one.)

Tannor[32] has explicitly considered in a time-dependent picture the case of resonance Raman scattering into final vibrational eigenstates in the ground state with odd quanta in an antisymmetric mode, such as the ν_3 mode in SO_2. One can reproduce the same ideas in a time-independent formalism. In the Kramers–Heisenberg–Dirac expression for the spontaneous resonance Raman scattering amplitude into a particular final state f in the ground electronic state, one writes,

$$\alpha_{fi}(\omega_I)=\sum_n \frac{\langle f|\boldsymbol{\mu}_{\text{down}}\cdot\mathbf{e}_S|n\rangle\langle n|\boldsymbol{\mu}_{\text{up}}\cdot\mathbf{e}_I|i\rangle}{E_i+\hbar\omega_I-E_n-i\hbar\Gamma}$$

Analysis of the up transition matrix element $\langle n|\boldsymbol{\mu}_{\text{up}}\cdot\mathbf{e}_I|i\rangle$ and the down transition matrix element $\langle f|\boldsymbol{\mu}_{\text{down}}\cdot\mathbf{e}_S|n\rangle$, in terms of symmetry constraints, proceeds the same for resonance Raman and dispersed fluorescence[34] (although for the latter you square each separately). In principle, you need to write each initial state $|i\rangle$, final state $|f\rangle$, and intermediate state $|n\rangle$ as a wavefunction with rotational, vibrational, and electronic parts and couplings. We now assume you can separate each into a product of a rotational part and a vibronic part, using the simplified notation for $|n\rangle$ of $|(r)_n(ve)_n\rangle$, making the assumption that Coriolis coupling can be neglected. We can factor out the rotational matrix elements of the operators that transform the ''up'' and ''down'' transition moments from space-fixed to the more convenient body-fixed coordinates, respectively. (Note: This leads to different rotational selection rules for up/down transitions that both use the same body-fixed component of the transition moment as compared to the selection rules for up/down transitions that use different components of the transition moment.) The strongly allowed ''up transition'' matrix element from the (0,0,0) vibrational eigenstate in the A_1 ground state would be via a b_2 component of the transition moment and would be of the form,

$$\langle(ve)_n|\boldsymbol{\mu}_{\text{up,body-fixed}}|(ve)_i\rangle=\langle a_1B_2|b_2|a_1A_1\rangle.$$

while Tannor[32] would also allow the nominally forbidden but vibronically allowed[34] up transition using an a_1 component of the dipole operator,

$$\langle(ve)_n|\boldsymbol{\mu}_{\text{up,body-fixed}}|(ve)_i\rangle=\langle b_2B_2|a_1|a_1A_1\rangle.$$

If the former is followed by an electronically forbidden but vibronically allowed emission step (i.e., $\langle b_2A_1|a_1|a_1B_2\rangle$) or the latter is followed by an electronically allowed emission step, $\langle b_2A_1|b_2|b_2B_2\rangle$, so the up and down transitions have used different components of the transition moment in each two-step process, then one can have odd quanta in the antisymmetric stretch mode in the final state in the ground state. Of course, Brand *et al.*[27] and others[35] considered exactly this in the analysis of their spectra, but Brand *et al.* discarded it as a possibility because the emission into bands with odd quanta in ν_3'' were just as strong as the emission into bands with even quanta in ν_3''. One can easily see from the assigned regions of the absorption spectrum[12] that the up transition is dominated by the contribution from the $\langle a_1B_2|b_2|a_1A_1\rangle$ matrix element, and so Brand *et al.* did not expect any bands (the odd ν_3 ones in this case) in the dispersed emission spectrum requiring an electronically forbidden but vibronically allowed absorption or emission step to be competitive with the fully electronically allowed emission into states with even quanta in ν_3''.[27] Their paper notes that since their spectra evidence comparable intensities in both even and odd final states, they discounted ''the possibility that the odd-ν_3'' bands belonged to a vibronically allowed subsystem of this strong electronic transition.''

We now propose a mechanism by which both the absorption and the emission step reaching states with odd quanta in ν_3'' could be strongly allowed, and thus competitive with the bands with even quanta in ν_3''. Consider the case where the resonant intermediate scattering eigenstate $|n\rangle$ is strongly mixed in character; we will write it as ''mixed b_2A_1/a_1B_2,'' but that the electronic character is largely B_2 in the Franck–Condon region of the excited state at geometries near the symmetric equilibrium ground-state geometry. Then the dominant matrix element for the absorption step would be $\langle$mixed $\mathbf{a_1B_2}/b_2A_1|b_2|a_1A_1\rangle$. Then, if the intermediate scattering eigenstate includes amplitude at very different geometries on the excited state potential energy surface, where the electronic configuration is an admixture of the ones having B_2 and A_1 symmetry in C_{2v}, there would be two allowed emission steps, $\langle a_1A_1|b_2|$ mixed $\mathbf{a_1B_2}/b_2A_1\rangle$ leading to even quanta in ν_3'' and $\langle b_2A_1|a_1|$ mixed

$a_1B_2/\mathbf{b_2A_1}\rangle$ leading to odd quanta in ν_3''. (We boldface the component of the mixed intermediate state which makes the transition strong in each case. This mechanism requires the A_1 electronic character in the intermediate state to have a strongly allowed electronic transition via the a_1 component of the transition moment to the A_1 ground electronic state, but SO_2 does indeed have such a $^1A_1$ excited state energetically proximate to the $^1B_2$ state at some geometries.[13,14] In Sec. IV below we argue that because the state with electronic configuration corresponding to the $1\,^1B_2$ state mixes and splits with a repulsive electronic configuration state of $^1A_1$ symmetry at an avoided curve crossing at C_s geometries along the S–O bond fission reaction coordinate, that this provides an adiabat with exactly the mixed electronic character required of the intermediate scattering state to observe strong emission into vibrational states with odd quanta in ν_3''.

It is worth looking at the spectra once more to see if they support the ideas presented thus far. We have shown that emission into final states with odd quanta in ν_3'' can have comparable intensity to emission into final states with even quanta in ν_3'', but if the odd quanta occur via a $\langle b_2A_1|a_1|$ mixed $a_1B_2/\mathbf{b_2A_1}\rangle$ emission step and the even quanta occur via a $\langle a_1A_1|b_2|$ mixed $\mathbf{a_1B_2}/b_2A_1\rangle$ emission step, we would expect some systematic differences in the odd-ν_3'' versus even-ν_3'' intensities in the spectra. Indeed, in the top three spectra in Fig. 1, one only sees strong emission bands with odd $(n=1)$ quanta in ν_3'', while at the excitation energies for the bottom two spectra in Fig. 1, one sees considerable emission into bands with both odd $(n=1)$ and even $(n=2)$ quanta in ν_3. The emission into odd quanta in ν_3'' have a higher intensity at the higher excitation energies, indicating that the contribution of b_2A_1 character in the intermediate scattering eigenstate at the three highest excitation energies in Fig. 1 must be relatively strong. Clearly, the admixture (into the nominal $^1B_2$ excited state) at nonsymmetric geometries of an excited electronic configuration that is $^1A_1$ in symmetry in C_{2v} geometries is more significant in the scattering eigenstates at higher excitation energies near 200 than at lower excitation energies near 210 nm, and is virtually absent in the intermediate scattering states excited at the longer wavelengths probed in Myers and Yang's[26] emission spectra.

IV. DISCUSSION

A. Predissociation mechanism near 200 nm

Most theoretical and experimental studies of SO_2's $\tilde{C}$ state predissociation concur that internal conversion to the ground electronic state is the dominant predissociation mechanism near the onset of the predissociation. However, some experimental studies support the coexistence of a predissociation mechanism via a repulsive triplet state of $^3A_1$ symmetry in C_{2v}, while theoretical studies also offer the possibility of a predissociation via a repulsive singlet state of $^1A_1$ symmetry in C_{2v}. The experimental evidence for the triplet channel is not all consistent, however. Kawasaki *et al.*[10] attributes the high kinetic energy distribution of the SO+O products from the 193-nm photodissociation to an exit barrier, proposing that the crossing with the repulsive triplet invoked by Kanamori *et al.*[11] would provide such a potential with such an exit barrier. However, Ebata *et al.*[5] present evidence for intersystem crossing they also believe consistent with Kanamori's results, but occurring near the onset of predissociation, contradicting a 2500-cm^{-1} exit barrier.

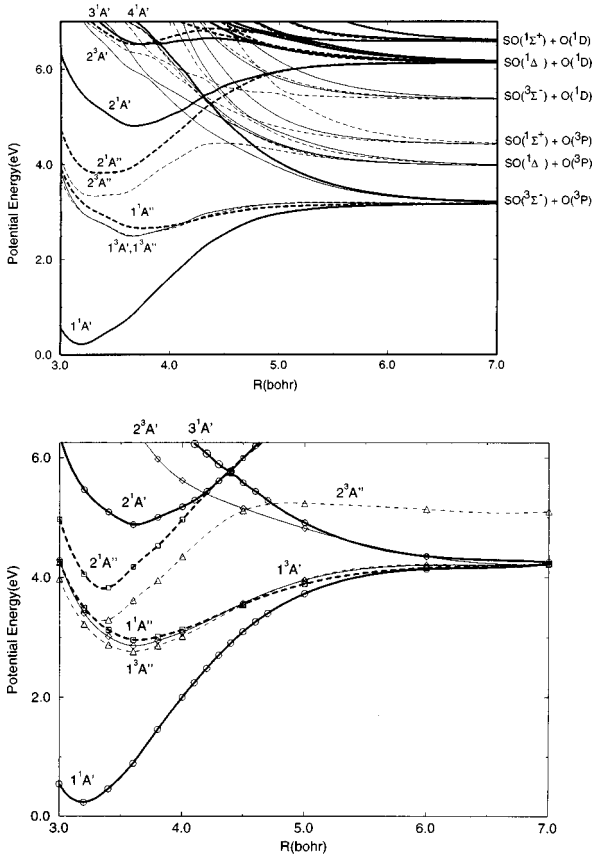

FIG. 4. (Top) CASSCF potential energy curves adapted from Ref. 14 for the low-lying electronic states of SO_2 involved in the photodissociation via the $\tilde{C}$ state, plotted as a function of the Jacobi coordinate R, with $\gamma=120°$ and $r=2.706a_0$. (bottom) More accurate MRCI curves from Ref. 14. Note that the energetics of the SO+O asymptotes in the CASSCF calculation are terrible, as noted by those authors. (Adapted from Ref. 14, Copyright 1997, with permission from Elsevier Science.)

Let us now analyze the dominant electronic character of these excited states of SO_2 in the vertical region and at stretched S–O bond distances. (Note that avoided crossings also occur as the O–S–O bond angle is changed.) We will use that background to ascertain what our emission spectra are telling us. The CASSCF and more accurate MRCI potential energy curves of Katagiri *et al.*[14] are shown in Fig. 4 (top) and (bottom), respectively, as a function of the Jacobi coordinate R. We care about the orbital character of the configuration states at the singlet avoided crossing because our emission spectra evidence a signature from configuration interaction mixing with an optically bright (transition to the ground electronic state) $^1A_1$ electronic configuration. The $2\,^1A'/3\,^1A'$ avoided crossing in C_s geometry at $R=4.3\,a_0$ in Fig. 4 (top) and at $R=4.4\,a_0$ in Fig. 4 (bottom) is formed from a curve crossing between the $^1B_2$ configuration state and a repulsive $^1A_1$ configuration state. Figure 4 (top) shows that the repulsive $^1A_1$ configuration state is not the $3\,^1A'$

TABLE I. GAUSSIAN 94 calculations (Ref. 36) of the $^1B_2$ and lowest two $^1A_1$ excited states of SO_2 using the equilibrium ground-state geometry of Herzberg ($R_{S-O}=1.4319$ Å, OSO angle$=119.5°$). The configuration interaction with single excitations (CIS) *ab initio* calculations (with a restricted Hartree–Fock reference determinant) were done with a 6-311+G* basis.

Electronic state	Vertical excitation energy (eV)	Oscillator strength
$\tilde{C}\ ^1B_2$	6.9319	0.1336
$2\ ^1A_1$	9.9016	0.0290
$3\ ^1A_1$	10.5488	0.1625

$(=2^1A_1)$ in the vertical region, but rather corresponds to a higher $^1A_1$ configuration state in the vertical region [since there are again avoided configuration crossings between the $3\ ^1A'$ and the $4\ ^1A'$ states apparent in Fig. 4 (top)]. Table I shows our GAUSSIAN 94 calculations[36] of the oscillator strengths to the $\tilde{C}\ ^1B_2$, $2\ ^1A_1$, and $3\ ^1A_1$ states at the vertical geometry. Indeed, the $3\ ^1A_1$ state (the one that appears to have the same orbital character as that of the repulsive singlet state involved in the avoided crossing with the $\tilde{C}$ state at nonsymmetric geometries) has considerable oscillator strength, comparable to that of the $\tilde{C}$ state. This is thus the only candidate, and a consistent one, for the A_1 configuration state which is making the emission to odd-ν_3'' in our emission spectra so strong for excitation energies near 200 nm (the repulsive triplet state would not have a strongly allowed optical transition to the singlet ground state).

The data and analysis presented thus far provide the first strong experimental evidence for the predissociation mechanism of the $\tilde{C}$ state via the repulsive $^1A_1$ state of SO_2. Let us review. The detailed analysis of our emission spectra in Sec. III above showed that at excitation energies near 200 nm the nominal $\tilde{C}\ ^1B_2$ state of SO_2 evidenced coupling to an excited electronic state that has A_1 character in C_{2v}. We showed that this must be an admixture of such a bright state into the resonant scattering wavefunction on the $2\ ^1A'$ adiabatic surface ($\tilde{C}\ ^1B_2$ in C_{2v}) that made the emission into final states with odd quanta in ν_3'' allowed. We propose that this $^1A_1$ configuration making the emission step bright is the repulsive $^1A_1$ configuration state that undergoes an avoided electronic curve crossing with the $\tilde{C}\ ^1B_2$ state as shown in Fig. 4. That contribution to the emission is small near the onset to predissociation and moderate near the 210-nm excitation wavelengths, but strong near 200 nm. Our excitation energy dependence implies the avoided crossing seam between the $^1B_2$ and the repulsive $^1A_1$ configuration states when they mix and split at non-C_{2v} geometries is accessed only at the higher excitation energies near 200 nm. Now we will look at what further *ab initio* evidence there is on the singlet avoided crossing seam.

Figure 5 shows Katagiri *et al.*'s calculated crossing seams (varying the R and γ Jacobi coordinates) when one S–O bond length is fixed at 2.706 a_0 between the $\tilde{C}$ state and the repulsive $^1A_1$ and $^3A_1$ states at non-C_{2v} geometries. The avoided crossing pseudoseam between the $2\ ^1A'$ and $3\ ^1A'$ singlet surfaces is at somewhat higher energies than the triplet seam, suggesting the predissociation mechanism via the

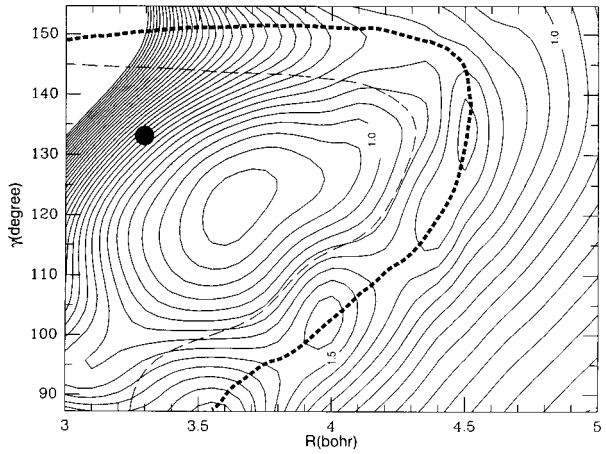

FIG. 5. A contour map of Katagiri *et al.*'s MRCI potential energy surface for the $2\ ^1A'$ state ($=\tilde{C}\ ^1B_2$ in the Frank–Condon region). The thick broken lines show the singlet pseudoseam formed by the avoided crossing with the repulsive singlet state that has $^1A_1$ symmetry in C_{2v}. The thin broken line shows the crossing seam with the repulsive triplet state that has $^3A_1$ symmetry in C_{2v}. The solid dot shows the Franck–Condon point for the $\tilde{C} \leftarrow \tilde{X}$ transition from $\tilde{X}(0,0,0)$. (Reproduced from Ref. 14, Copyright 1997, with permission from Elsevier Science.)

repulsive singlet would turn on at higher excitation energies than the predissociation via the repulsive triplet (at lower excitation energies, they conclude that internal conversion to the ground state is the predominant predissociation mechanism). They largely discount the repulsive singlet mechanism because they find the singlet avoided crossing is only very narrowly avoided, only by 20 meV at $\gamma=120°$. However, let us consider exciting the molecule around 190 or 200 nm near the peak of the SO_2 absorption spectrum. One can crudely think of the dynamics as being represented by starting a classical trajectory from the Franck–Condon region shown by the solid dot in Fig. 5. The force the molecule feels in the Franck–Condon region drives the classical trajectories both to smaller γ and to larger R, consistent with the activity in the bend and in ν_3 in our emission spectra excited near 200 nm. Assuming the concurrent changes in the bound S–O internuclear distance r does not change the forces along R and γ too much, such a group of trajectories would reach the avoided crossing seam at angles near 100°, where Katagiri *et al.* find the avoided crossing is more strongly avoided, as large as 0.1 eV near $\gamma=90°$. In a two-state Landau–Zener model, such a splitting at the avoided crossing of 800 cm^{-1} is large enough to allow a significant fraction of the trajectories to evolve adiabatically through the avoided crossing (although the probability of a diabatic traversal of the avoided crossing, where the wavefunction retains the parent $^1B_2$ orbital configuration and the nuclear dynamics hops to the bonding region on the $3\ ^1A'$ potential energy surface (PES) as it traverses the avoided crossing, is not negligible). Thus the portion of the time-independent scattering wavefunction excited near 200 nm that corresponds to the adiabatic traversal of the avoided crossing by necessity develops 50/50 character of the repulsive $^1A_1$ orbital configuration at the avoided crossing seam, and we propose it is this character in the mixed state that allows the strong emission into odd-ν_3'' in our emission spectra excited near 200 nm.

Thus, our spectra offer the first strong experimental evidence for the opening of a predissociation channel via an avoided crossing with a repulsive singlet state. It may well be that some of the photofragments in Kawasaki *et al.*'s[10] photodissociation experiment at 193 nm result from this predissociation mechanism. Their measured photofragment kinetic energy distribution indicated recoil on a potential energy surface with a 2500-cm^{-1} exit barrier as measured from the $SO(^3\Sigma^-)+O(^3P)$ asymptote. If one adds the 9700 cm^{-1} energy of the singlet avoided crossing pseudoseam (estimated by Katagiri *et al.*) to the 45 400 cm^{-1} value for the onset of predissociation (as a measure of the asymptote's energy), one would conclude that the pseudoseam is just above being energetically allowed at 193 nm. Either the energetics of the MRCI calculations are in error by several tenths of an eV or we are sensitive to the admixing of the singlet repulsive configuration into the $^1B_2$ electronic configuration even at energies below the true avoided crossing (this is actually to be expected). Finally, we note that because the predissociation mechanism via the repulsive triplet is to an optically dark state, the opening of this mechanism, presumably at somewhat lower excitation energies, is not probed in our emission spectrum.

There is one difficult point one must consider when one discusses the component of the transition moment which is bright in the emission spectrum for even or odd ν_3''. We have invoked both A_1 and B_2 electronic character at the avoided crossing seam, where the mixed character simply results from the configuration interaction between electronic configurations that undergo an avoided crossing. However, we have been labeling the two contributions to the electronic character (and the components of the dipole moment for the transition from each to the ground electronic state) with global C_{2v} symmetry labels, even though the crossing is only avoided at nonsymmetric geometries. This is only correct for symmetrical molecules like H_2S, SO_2, and NO_2. Using the C_{2v} symmetry label to describe the electronic character of a wavefunction even when it samples distorted nonsymmetric geometries is described in detail in Refs. 32 and 33. [One identifies the full symmetry of $\psi_e(r,R)$ with $S\psi_e(r,R) = D^e(S)\psi_e(r,R)$, where S is some symmetry operation belonging to the point group of the molecule (in this case C_{2v}) and $D^e(S)$ is the character in the irreducible representation to which $\psi_e(r,R)$ belongs, but S does not have the same effect on electrons and nuclei. Tannor describes that if S is a reflection operation, S reflects the electrons through an appropriate reflection plane while it reflects and then permutes back the nuclei.] We only add here that it is not, as Ref. 32 implies, applicable to Born–Oppenheimer electronic wavefunctions, but only to diabatic electronic wavefunctions (at least diabatic with respect to orbital changes that mix orbitals of different global C_{2v} symmetry). One can easily see this by considering the upper b_2 orbital of the valence excited state (A_2 in C_{2v}) of H_2S depicted in Fig. 5 of Ref. 31. One can easily identify the global C_{2v} symmetry of this orbital, even at nonsymmetric geometries, using the prescription above, but in the Born–Oppenheimer electronic wavefunction when the upper orbital is from a mixed Rydberg/valence electronic state at nonsymmetric geometries one cannot. [The upper orbital in the Rydberg B_1 electronic configuration has global a_1 symmetry, so the upper orbital is mixed at nonsymmetric geometries and no longer has a C_{2v} global symmetry (the lower orbital in both electronic configurations is an out-of-plane p orbital on the sulfur atom, so is b_1)]. However, the upper orbitals and common lower orbital in both the Rydberg and the valence diabatic electronic configuration each have identifiable global C_{2v} symmetry, thus we apply the global C_{2v} symmetry labels only to the component diabatic character in a mixed Born–Oppenheimer wavefunction, not to the whole Born–Oppenheimer electronic wavefunction.

B. Future work

Two key measurements are suggested by the results reported here. First, if the absorption and the emission steps utilize two different components of the transition moment for the odd-ν_3'' bands, but the same component of the transition moment for the even-ν_3'' bands, the angular distribution and the polarization of the emitted photons should be different for the odd-ν_3'' versus the even-ν_3'' bands if the predissociation times are short enough to limit the smearing from molecular rotation.[32,37–39] Tannor[32] has discussed this in some detail for SO_2, and Harris *et al.*[39] and Butler *et al.*[37] have considered an analogous situation where they also consider potential interference terms in the resonance Raman scattering process (but only if the absorption step is also bright with both components of the transition moment). We plan to pursue this polarization measurement on SO_2 near 200-nm excitation wavelengths. Second, a more difficult experiment to pursue, because of the dearth of high power tunable light sources in this wavelength range, is the tunable photofragmentation of SO_2 from 210 through 180 nm to detect the opening of the predissociation channel via the repulsive singlet. We also hope to interest our theoretical colleagues in the multisurface resonance Raman scattering calculation of SO_2 near 200 nm, as it offers the chance to probe avoided crossings via the appearance of what workers have traditionally called ''nominally forbidden'' transitions, but which are in fact fully allowed due to configuration interaction at an avoided electronic curve crossing.

ACKNOWLEDGMENTS

This work was supported by the Division of Chemical Sciences, Office of Basic Energy Sciences, Office of Energy Research, U.S. Department of Energy, under Grant No. DE-FG02-92ER14305. We would like to thank A. Merer, J. L. Kinsey, and D. Levy for several helpful discussions. We are indebted to A. Merer for assigning the bands in our emission spectra.

[1] E. S. Barker, Geophys. Res. Lett. **6**, 117 (1979).
[2] A. I. Stewart, D. E. Anderson, Jr., L. W. Esposito, and C. A. Barth, Science **203**, 777 (1979).
[3] R. R. Conway, R. P. McRay, and C. A. Barth, Geophys. Res. Lett. **6**, 629 (1979).
[4] H. Okabe, J. Am. Chem. Soc. **93**, 7095 (1971).
[5] T. Ebata, O. Nakazawa, and M. Ito, Chem. Phys. Lett. **143**, 31 (1988).
[6] M.-H. Hui and S. A. Rice, Chem. Phys. Lett. **17**, 474 (1972).
[7] M. Ivanco, J. Hager, W. Sharfirm, and S. C. Wallace, J. Chem. Phys. **78**, 6531 (1983).

[8] H. Abe and H. Hayashi, Chem. Phys. Lett. **187**, 227 (1991).
[9] D. E. Freeman, K. Yoshino, J. R. Esmold, and W. H. Parkinson, Planet. Space Sci. **32**, 1125 (1984).
[10] (a) M. Kawasaki, K. Kasatani, H. Sato, H. Shinohara, and N. Nishi, Chem. Phys. **73**, 377 (1982); (b) M. Kawasaki and H. Sato, Chem. Phys. Lett. **139**, 585 (1987).
[11] H. Kanamori, J. E. Butler, K. Kawaguchi, C. Yamada, and E. Hirota, J. Chem. Phys. **83**, 611 (1985).
[12] A. Okazaki, T. Ebata, and N. Mikami, J. Chem. Phys. **107**, 8752 (1997).
[13] K. Kamiya and H. Matsui, Bull. Chem. Soc. Jpn. **64**, 2792 (1991).
[14] H. Katagiri, T. Sako, A. Hishikawa, T. Yazaki, K. Onda, K. Yamanouchi, and K. Yoshino, J. Mol. Struct. **413**, 589 (1997).
[15] Y.-L. Huang and R. J. Gordon, J. Chem. Phys. **93**, 868 (1990).
[16] P. Felder, C. S. Effenhauser, B. M. Haas, and J. R. Huber, Chem. Phys. Lett. **148**, 417 (1988).
[17] A. Freedman, S.-C. Yang, R. Bersohn, and M. Kawasaki, J. Chem. Phys. **70**, 5313 (1979).
[18] C. Braatz and E. Tiemann, Chem. Phys. **229**, 93 (1998), and references therein.
[19] S. Becker, C. Braatz, J. Lindner, and E. Tiemann, Chem. Phys. **196**, 275 (1995), and references therein.
[20] E. J. Heller, Acc. Chem. Res. **14**, 368 (1981).
[21] (a) S.-Y. Lee and E. J. Heller, J. Chem. Phys. **71**, 4777 (1979); (b) D. J. Tannor and E. J. Heller, *ibid.* **77**, 202 (1982).
[22] D. G. Imre, J. L. Kinsey, A. Sinha, and J. Krenos, J. Phys. Chem. **88**, 3956 (1984).
[23] B. R. Johnson, C. Kittrell, P. B. Kelly, and J. L. Kinsey, J. Phys. Chem. **100**, 7743 (1996).
[24] M. D. Person, K. Q. Lao, B. J. Eckholm, and L. J. Butler, J. Chem. Phys. **91**, 812 (1989).
[25] K. Q. Lao, M. D. Person, P. Xayariboun, and L. J. Butler, J. Chem. Phys. **92**, 823 (1990).
[26] T-S. Yang and A. B. Myers, J. Chem. Phys. **95**, 6207 (1991).
[27] (a) J. C. D. Brand, D. R. Humphrey, A. E. Douglas, and I. Zanon, Can. J. Phys. **51**, 530 (1973); (b) A. R. Hoy and J. C. D. Brand, Mol. Phys. **36**, 1409 (1978).
[28] R. D. Shelton, A. H. Nielson, and W. Fletcher, Can. J. Phys. **21**, 2178 (1953).
[29] E. A. Rohlfing and J. J. Valentini, J. Chem. Phys. **83**, 521 (1985).
[30] D. G. Imre, J. L. Kinsey, R. W. Field, and D. H. Katayama, J. Phys. Chem. **86**, 2564 (1982).
[31] See, P. W. Browning, E. Jensen, G. C. G. Waschewsky, M. R. Tate, L. J. Butler, and J. P. Hessler, J. Chem. Phys. **101**, 5652 (1994), and references therein.
[32] D. J. Tannor, J. Phys. Chem. **92**, 3341 (1988).
[33] P. R. Bunker, *Molecular Symmetry and Spectroscopy* (Academic, Orlando, FL, 1979), Chap. 11.
[34] G. Herzberg, *Electronic Spectra and Electronic Structure of Polyatomic Molecules* (Van Nostrand, Princeton, 1969), pp. 174–5 and 242.
[35] K. K. Innes, J. Mol. Spectrosc. **120**, 1 (1986).
[36] GAUSSIAN 94, Revision E.2, M. J. Frisch, G. W. Trucks, H. B. Schlegel, P. M. W. Gill, B. G. Johnson, M. A. Robb, J. R. Cheeseman, T. Keith, G. A. Petersson, J. A. Montgomery, K. Raghavachari, M. A. Al-Laham, V. G. Zakrzewski, J. V. Ortiz, J. B. Foresman, J. Cioslowski, B. B. Stefanov, A. Nanayakkara, M. Challacombe, C. Y. Peng, P. Y. Ayala, W. Chen, M. W. Wong, J. L. Andres, E. S. Replogle, R. Gomperts, R. L. Martin, D. J. Fox, J. S. Binkley, D. J. Defrees, J. Baker, J. P. Stewart, M. Head-Gordon, C. Gonzalez, and J. A. Pople, Gaussian, Inc., Pittsburgh, PA, 1995.
[37] M. R. Wedlock, E. Jensen, L. J. Butler, and K. F. Freed, J. Phys. Chem. **95**, 8096 (1991).
[38] R. D. Coalson and J. L. Kinsey, J. Chem. Phys. **85**, 4322 (1986).
[39] R. A. Harris, M. R. Wedlock, L. J. Butler, and K. F. Freed, J. Chem. Phys. **96**, 2437 (1992).